11th US NATIONAL CONGRESS
ON COMPUTATIONAL MECHANICS

Cohesive Zone Modeling of Dynamic Fracture: Adaptive Mesh Refinement and Coarsening

Glaucio H. Paulino[1], Kyoungsoo Park[2], Waldemar Celes[3], Rodrigo Espinha[3]

[1] Department of Civil and Environmental Engineering
University of Illinois at Urbana-Champaign

[2] School of Civil and Environmental Engineering
Yonsei University, Seoul, Korea

[3] Department of Computer Science
Pontifical Catholic University of Rio de Janeiro (PUC-Rio)


7/25/2011

Outline

- **Cohesive Zone Modeling**
- **Potential-Based Cohesive Model**
- **Adaptive Topological Operators**
- **Computational Examples**
  - Mode I pre-defined crack path
  - Mixed-mode fracture problem
  - Micro-Branching
- **Summary**

Cohesive Zone Modeling

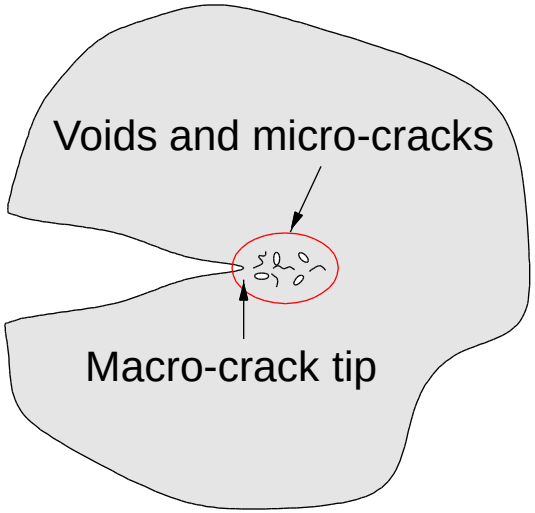

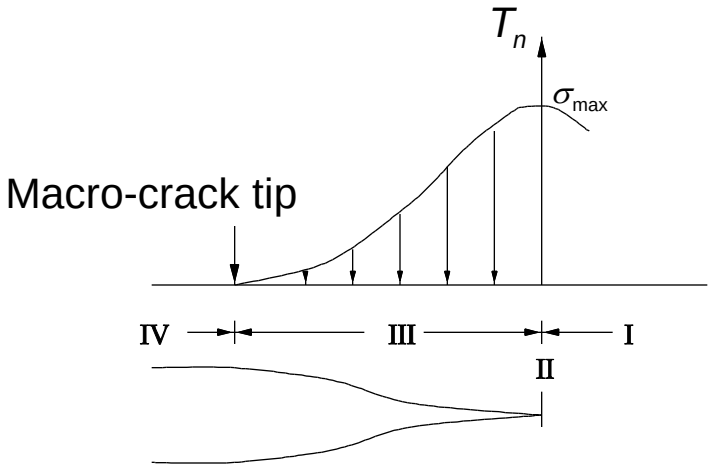

- **Constitutive Relationship of Cohesive Fracture**
  - Non-potential based-model vs. Potential based-model
- **Computational Methods**
  - Cohesive surface elements, enrichment functions, embedded discontinuities

Previous Potentials for Fracture

- **Needleman A. (1987)**
  - Polynomial potential / linear shear interaction
- **Needleman A. (1990)**
  - Exponential potential / periodic dependence
- **Beltz G.E. and Rice J.R. (1991)**
  - Generalized the potential (Exponential + Sinusoid)
- **Xu X.P. and Needleman A. (1993)**
  - Exponential potential (Exponential + Exponential)

- Needleman A. 1987, A continuum model for void nucleation by inclusion debonding, Journal of Applied Mechanics, 54, 525-531
- Needleman A. 1990, An analysis of tensile decohesion along an interface, Journal of the Mechanics and Physics of Solid, 3, 289-324
- Beltz GE and Rice JR, 1991, Dislocation nucleation versus cleavage decohesion at crack tip, Modeling the Deformation of Crystalline Solids, 457-480.
- Xu XP and Needleman, 1993, Void nucleation by inclusion debonding in a crystal matrix, Modeling Simulation Material Science Engineering, 1, 111-132.

Xu X.P. and Needleman A. (1993)

Xu XP and Needleman, 1993, Void nucleation by inclusion debonding in a crystal matrix, Modeling Simulation Material Science Engineering, 1, 111-132.

Cohesive Relationship

- Normal direction: Exponential → $T_n = \left[B(\Delta_t)\Delta_n - C(\Delta_t)\right]\exp(-\Delta_n / \delta_n)$
- Tangential direction: Exponential → $T_t = A(\Delta_n)\,\dfrac{\Delta_t}{\delta_t}\exp(-\Delta_t^{\,2} / \delta_t^{\,2})$
- Boundary Condition

$$\phi_n = \int_0^\infty T_n(\Delta_n, 0)\,d\Delta_n \qquad \phi_t = \int_0^\infty T_t(0, \Delta_t)\,d\Delta_t \qquad C(0) = 0$$

$$\lim_{\Delta n \to \infty} T_n(\Delta_n, \Delta_t) = 0 \qquad \lim_{\Delta n \to \infty} T_t(\Delta_n, \Delta_t) = 0 \qquad \lim_{\Delta t \to \infty} T_t(\Delta_n, \Delta_t) = 0 \qquad \lim_{\Delta t \to \infty} T_n(\Delta_n, \Delta_t) \neq 0$$

Introduce additional condition Δ_n^* instead of $\lim_{\Delta t \to \infty} T_n(\Delta_n, \Delta_t) = 0$

$$\lim_{\Delta_t \to \infty} T_n(\Delta_n^*, \Delta_t) = 0$$

$$\Psi(\Delta_n, \Delta_t) = \phi_n + \phi_n \exp\left(\frac{-\Delta_n}{\delta_n}\right)\left\{\left[1 - r + \frac{\Delta_n}{\delta_n}\right]\frac{(1-q)}{(r-1)} - \left[q + \frac{(r-q)}{(r-1)}\frac{\Delta_n}{\delta_n}\right]\exp\left(-\frac{\Delta_t^{\,2}}{\delta_t^{\,2}}\right)\right\}$$

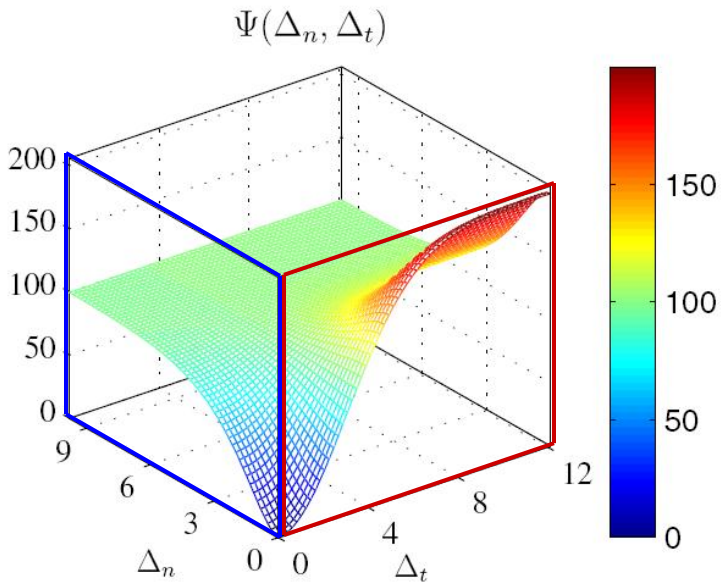

$$\phi_n = 100\,N/m$$
$$\phi_t = 200\,N/m$$
$$\sigma_{\max} = 30\,MPa$$
$$\tau_{\max} = 40\,MPa$$

$$r = \frac{\Delta_n^*}{\delta_n} = 0$$

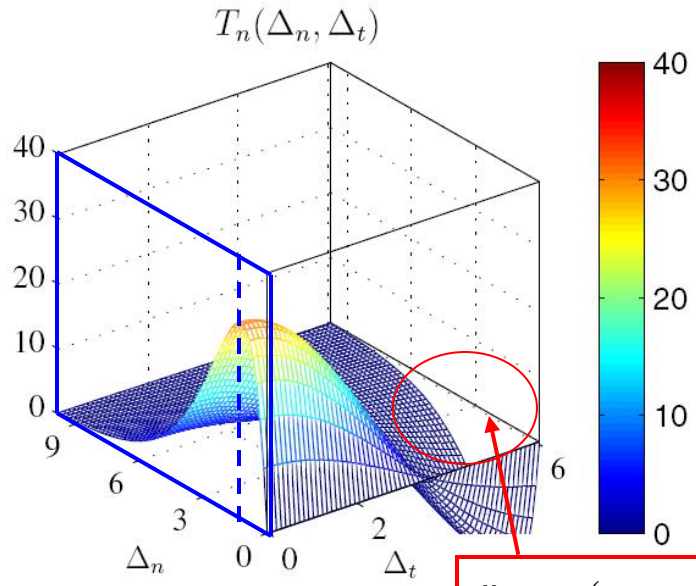

Mode I

$$\lim_{\Delta t \to \infty} T_n(\Delta_n, \Delta_t) < 0$$

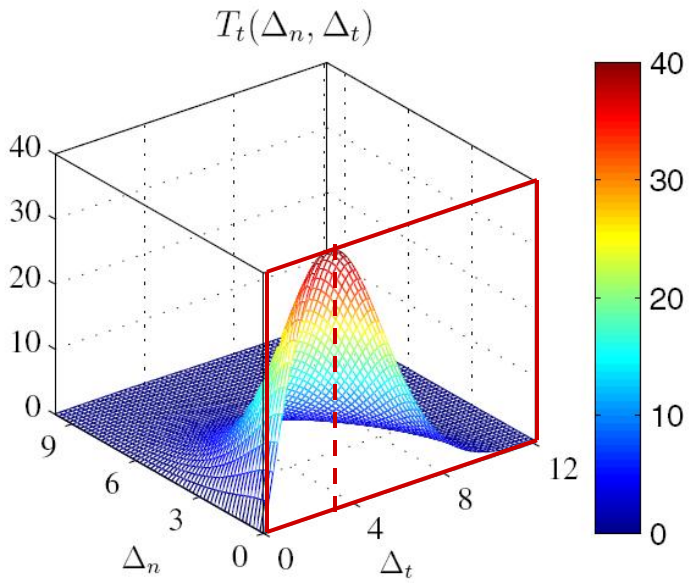

Mode II

Remarks

- **Previous Potential**
  - Boundary condition is not symmetric → $\lim_{\Delta t \to \infty} T_n(\Delta_n, \Delta_t) \neq 0$
  - Vague fracture parameter, r (or Δ_n^*) → Okay if fracture energies are the same
  - Complete separation at infinity
  - Could not control initial slope → Large compliance
- **Proposed Potential**
  - Expressed by a single function
  - Different fracture energy : ϕ_n, ϕ_t
  - Different cohesive strength : $\sigma_{\max}$, $\tau_{\max}$
  - Different cohesive relation: α, β
  - Different initial slope : λ_n, λ_t

Boundary Conditions

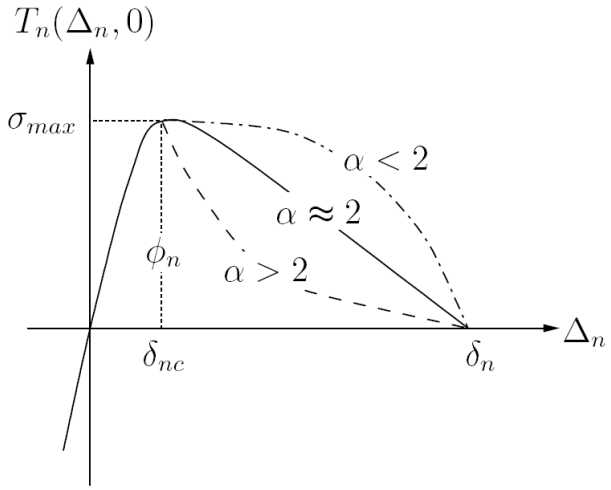

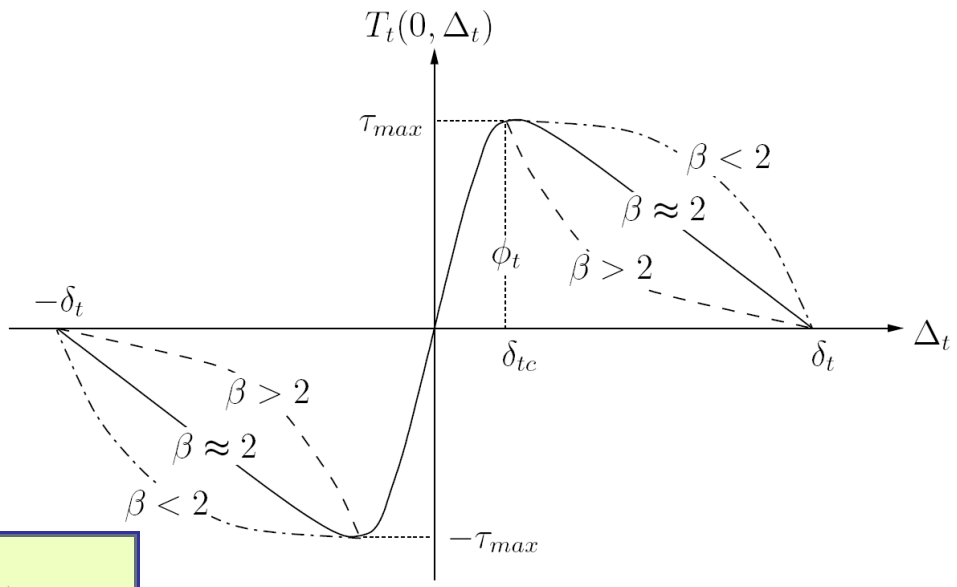

$$\phi_n = \int_0^{\delta_n} T_n(\Delta_n, 0)\mathrm{d}\Delta_n$$

$$\left.\frac{\partial T_n}{\partial \Delta_n}\right|_{\Delta_n=\delta_{nc}} = 0$$

$$T_n(\delta_{nc}, 0) = \sigma_{\max}$$

$$T_n(\delta_n, \Delta_t) = 0$$

$$T_n(\Delta_n, \bar{\delta}_t) = 0$$

$$\phi_t = \int_0^{\delta_t} T_t(0, \Delta_t)\mathrm{d}\Delta_t$$

$$\left.\frac{\partial T_t}{\partial \Delta_t}\right|_{\Delta_t=\delta_{tc}} = 0$$

$$T_t(0, \delta_{tc}) = \tau_{\max}$$

$$T_t(\Delta_n, \delta_t) = 0$$

$$T_t(\bar{\delta}_n, \Delta_t) = 0$$

Various material behavior, i.e.

Plateau-type $1 < \alpha, \beta << 2$

Brittle material $\alpha, \beta \approx 2$

Quasi-brittle material $\alpha, \beta >> 2$

PPR: Unified Mixed Mode Potential

$$\Psi(\Delta_n, \Delta_t) = \min(\phi_n, \phi_t) + \left[\Gamma_n \left(1 - \frac{\Delta_n}{\delta_n}\right)^{\alpha} \left(\frac{m}{\alpha} + \frac{\Delta_n}{\delta_n}\right)^{m} + \langle \phi_n - \phi_t \rangle\right] \left[\Gamma_t \left(1 - \frac{|\Delta_t|}{\delta_t}\right)^{\beta} \left(\frac{n}{\beta} + \frac{|\Delta_t|}{\delta_t}\right)^{n} + \langle \phi_t - \phi_n \rangle\right]$$

- **Fracture energy**
- **Cohesive strength**
- **Cohesive interaction shape**
- **Initial slope**

- **Energy Constants: Γ_n and Γ_t**
- **Exponents: *m* and *n***
- **Characteristic length scales: δ_n and δ_t**
- **Shape parameters : α and β**

K. Park, GH. Paulino, JR. Roesler, 2009, A unified potential-based cohesive model of mixed-mode fracture, *Journal of the Mechanics and Physics of Solids* 57, 891-908.

Extension for the *EXTRINSIC* Model

- **Correct Limit Procedure**
  - Limit of initial slope indicators in the potential

$$\Psi(\Delta_n, \Delta_t) = \min(\phi_n, \phi_t) + \left[\Gamma_n \left(1 - \frac{\Delta_n}{\delta_n}\right)^{\alpha} + \langle \phi_n - \phi_t \rangle\right] \left[\Gamma_t \left(1 - \frac{|\Delta_t|}{\delta_t}\right)^{\beta} + \langle \phi_t - \phi_n \rangle\right]$$

  - Energy constants: Γ_n and Γ_t
  - Characteristic length scales: δ_n and δ_t
  - Shape parameters: α and β
- **Exclude elastic behavior → Extrinsic model**
- **Consider different fracture energy:** ϕ_n, ϕ_t
- **Describe different cohesive strength:** σ_{max}, τ_{max}
- **Represent various cohesive shape:** α, β

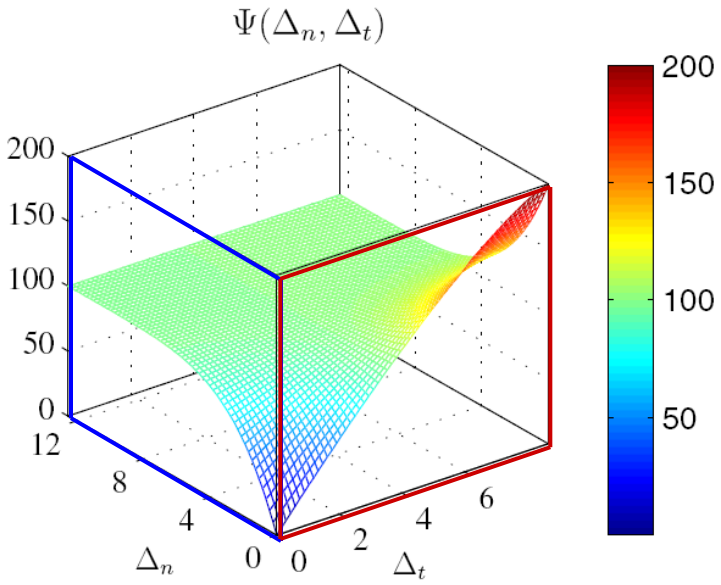

$\phi_n = 100 N/m$	$\phi_t = 200 N/m$
$\sigma_{\max} = 40 MPa$	$\tau_{\max} = 30 MPa$
$\alpha = 5$	$\beta = 1.3$

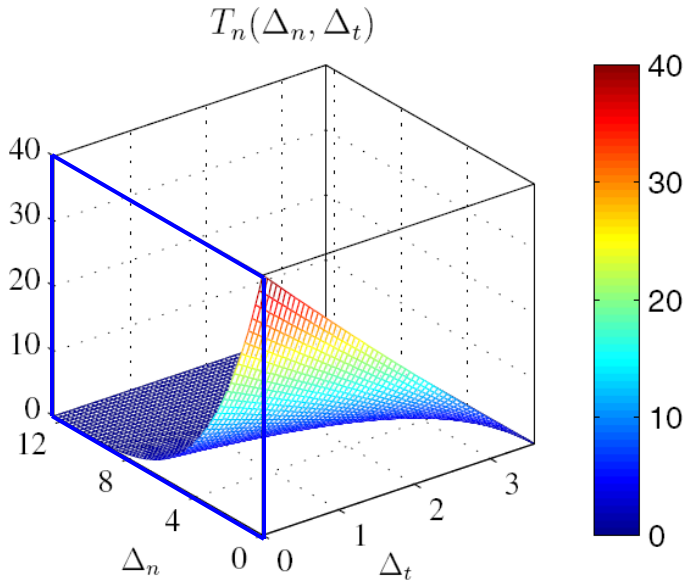

Mode I

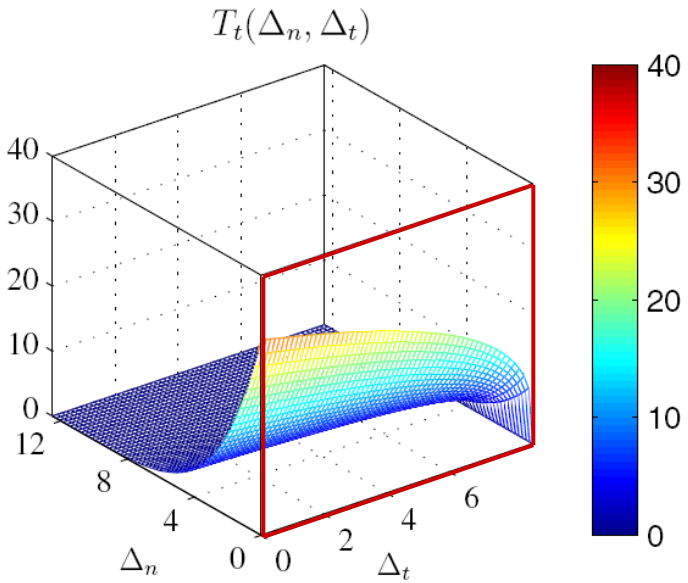

Mode II

Topological Operators

- **Nodal Perturbation**

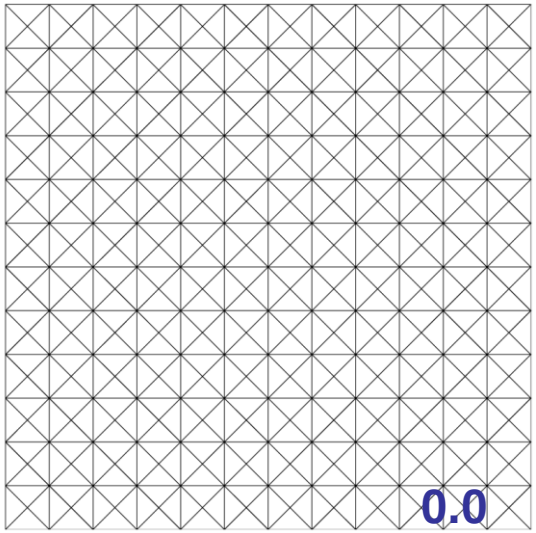

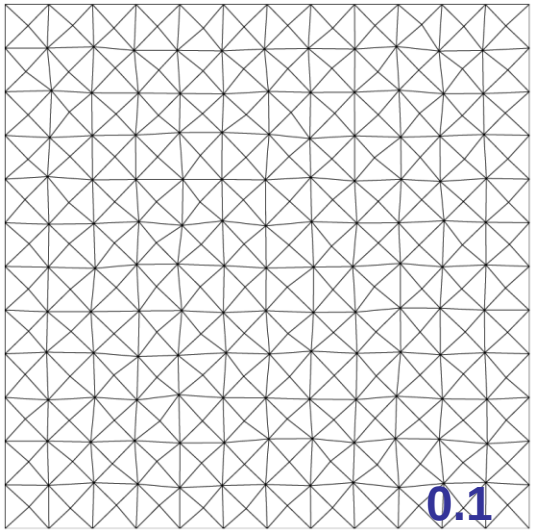

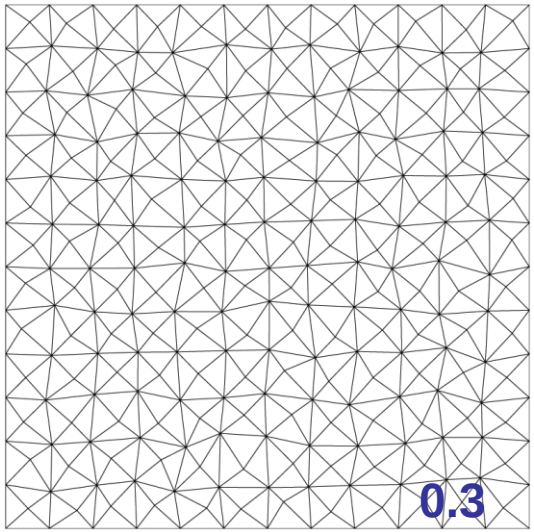

- **Edge-Swap**

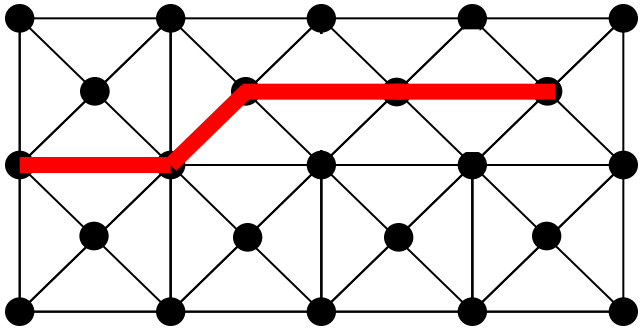

G.H. Paulino, K. Park, W. Celes, and R. Espinha, 2010, Adaptive dynamic cohesive fracture simulation using edge-swap and nodal perturbation operators, *International Journal for Numerical Methods in Engineering* 84, 1303-1343.

Topological Operators

- **Edge-Split**
  - Adaptive mesh refinement based on *a priori* knowledge

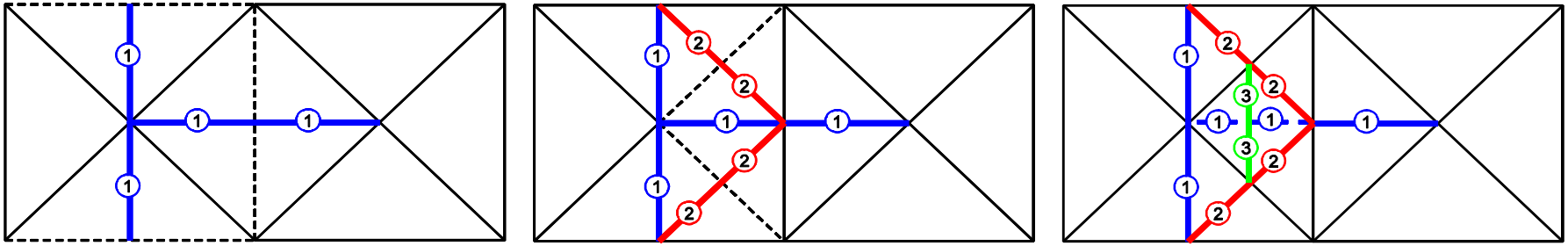

- **Vertex-Removal (or Edge-Collapse)**
  - Adaptive mesh coarsening based on *a posteriori* error estimation, i.e. root mean square of strain error

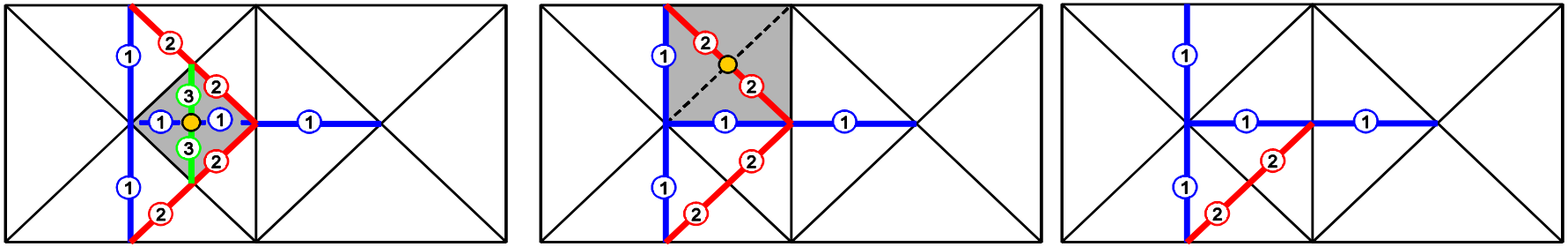

K. Park, G.H. Paulino, W. Celes, and R. Espinha, 2010, Adaptive mesh refinement and coarsening for cohesive dynamic fracture, *International Journal for Numerical Methods in Engineering* (in press).

Adaptive Mesh Coarsening

Coarsening Criterion

$$e_{4k} = \left[\sum_{i=1}^{4} \frac{\int_{\Omega_i} (\overline{\boldsymbol{\epsilon}}_{\mathrm{f}} - \overline{\boldsymbol{\epsilon}}_{\mathrm{c}})^T (\overline{\boldsymbol{\epsilon}}_{\mathrm{f}} - \overline{\boldsymbol{\epsilon}}_{\mathrm{c}}) d\Omega}{\Omega_i} \right]^{1/2}$$

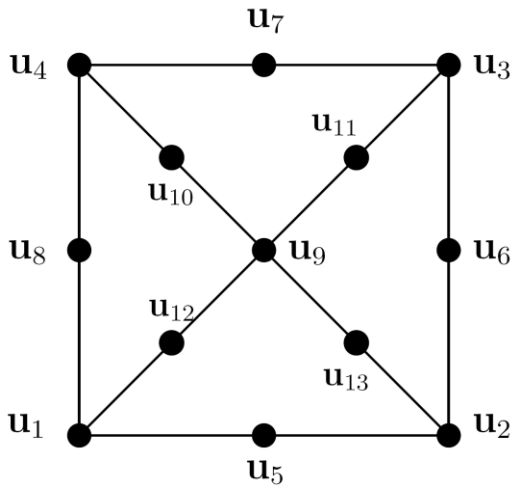

Local Update

$$\min \|\mathbf{u}_9 - \widetilde{\mathbf{u}}_9\|^2$$

$$g(\widetilde{\mathbf{u}}_9) = E_{\mathrm{int}} - \widetilde{E}_{\mathrm{int}}(\widetilde{\mathbf{u}}_9) = 0$$

$$E_{\mathrm{int}} = E_{\mathrm{int}(x)} + E_{\mathrm{int}(y)}$$

$$\widetilde{E}_{\mathrm{int}}(\widetilde{\mathbf{u}}_9) = \widetilde{E}_{\mathrm{int}(x)}(\widetilde{\mathbf{u}}_9) + \widetilde{E}_{\mathrm{int}(y)}(\widetilde{\mathbf{u}}_9)$$

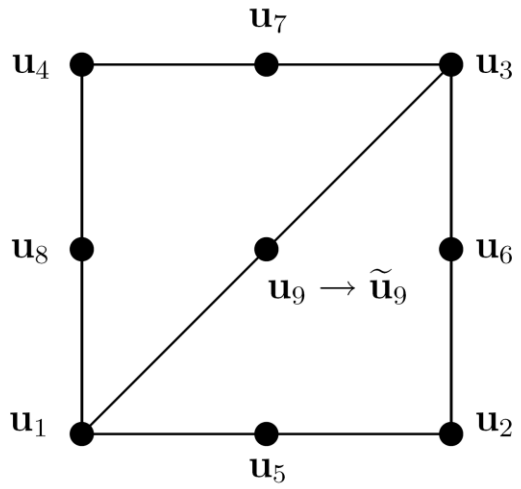

Mode I Pre-defined Crack Propagation

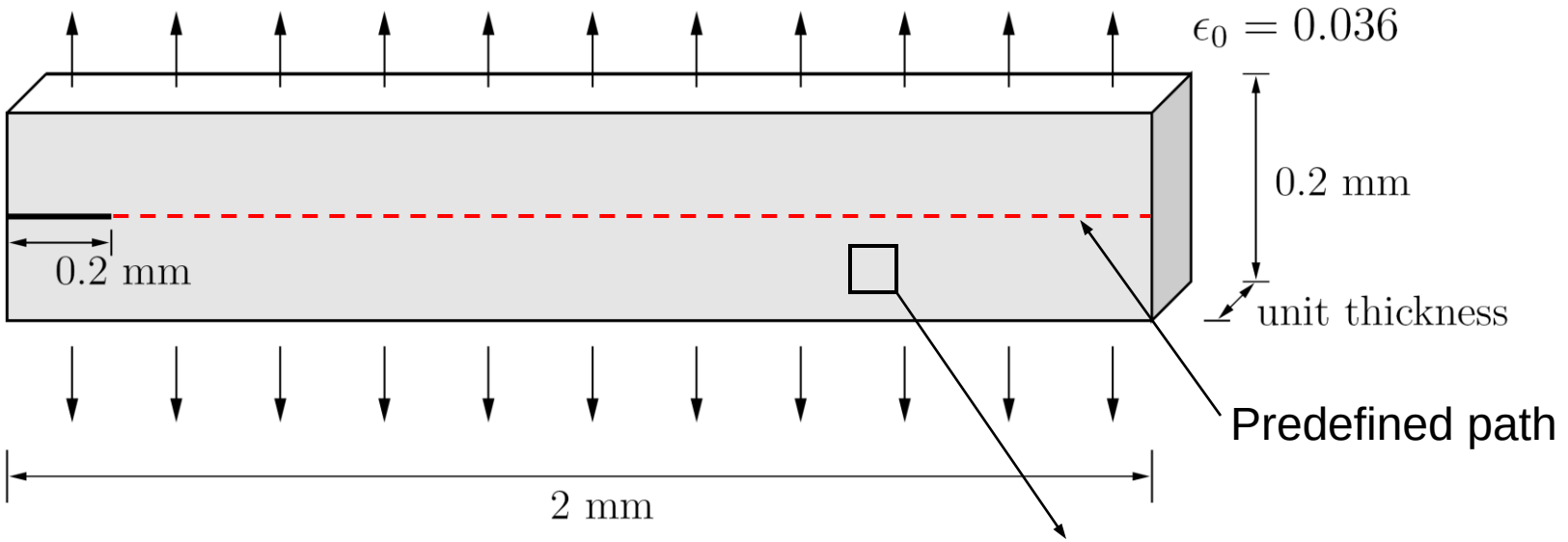

E	v	ρ	G_I	T_{max}
3.24 GPa	0.35	1190 kg/m^3	352 N/m	324 MPa

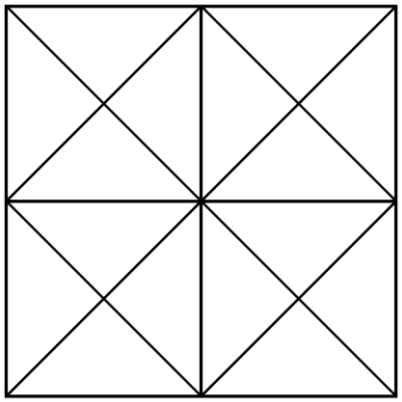

4k mesh

Computational Results

- **Uniform Mesh Refinement**
  - 400x40 mesh grid
  - Element size: 5μm
  - 64000 elements, 128881 nodes
- **Adaptive Mesh Refinement**
  - 100x10 mesh grid
  - Element size: 20~5μm
  - 4448 elements, 9147 nodes

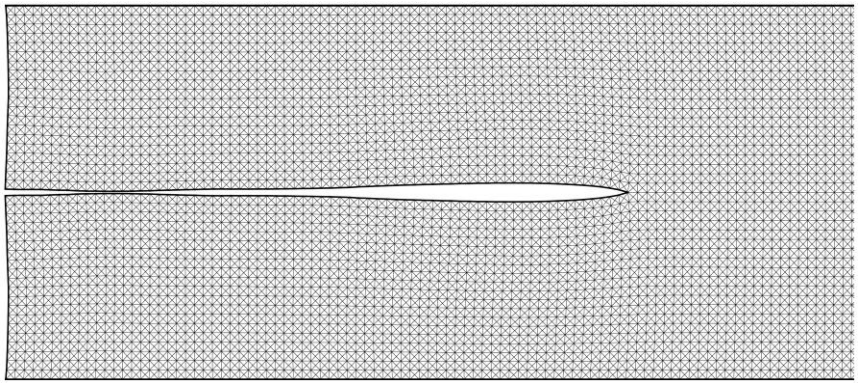

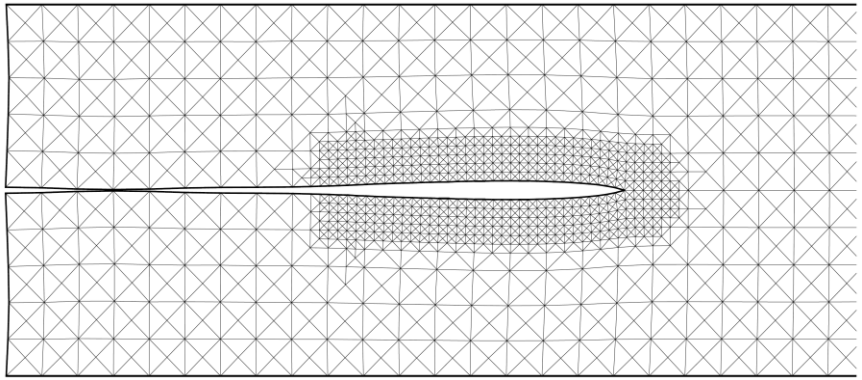

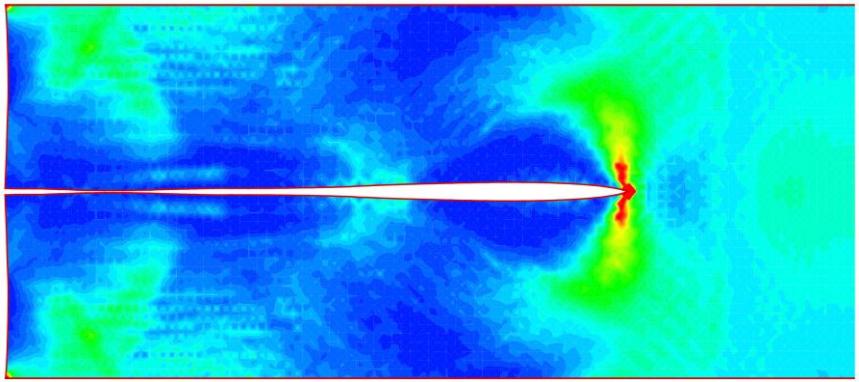

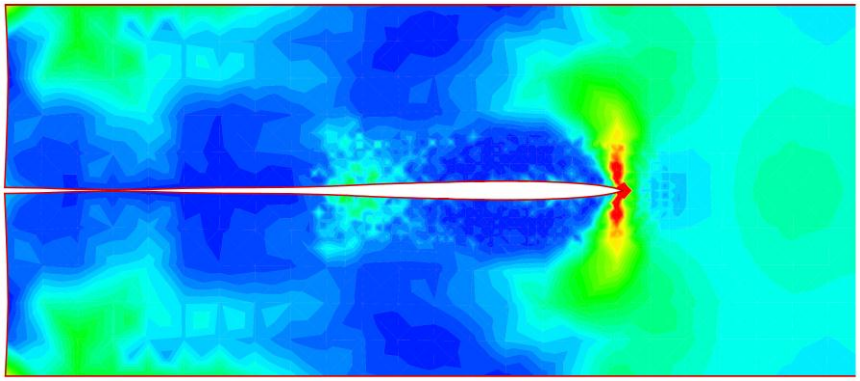

Computational Results (AMR)

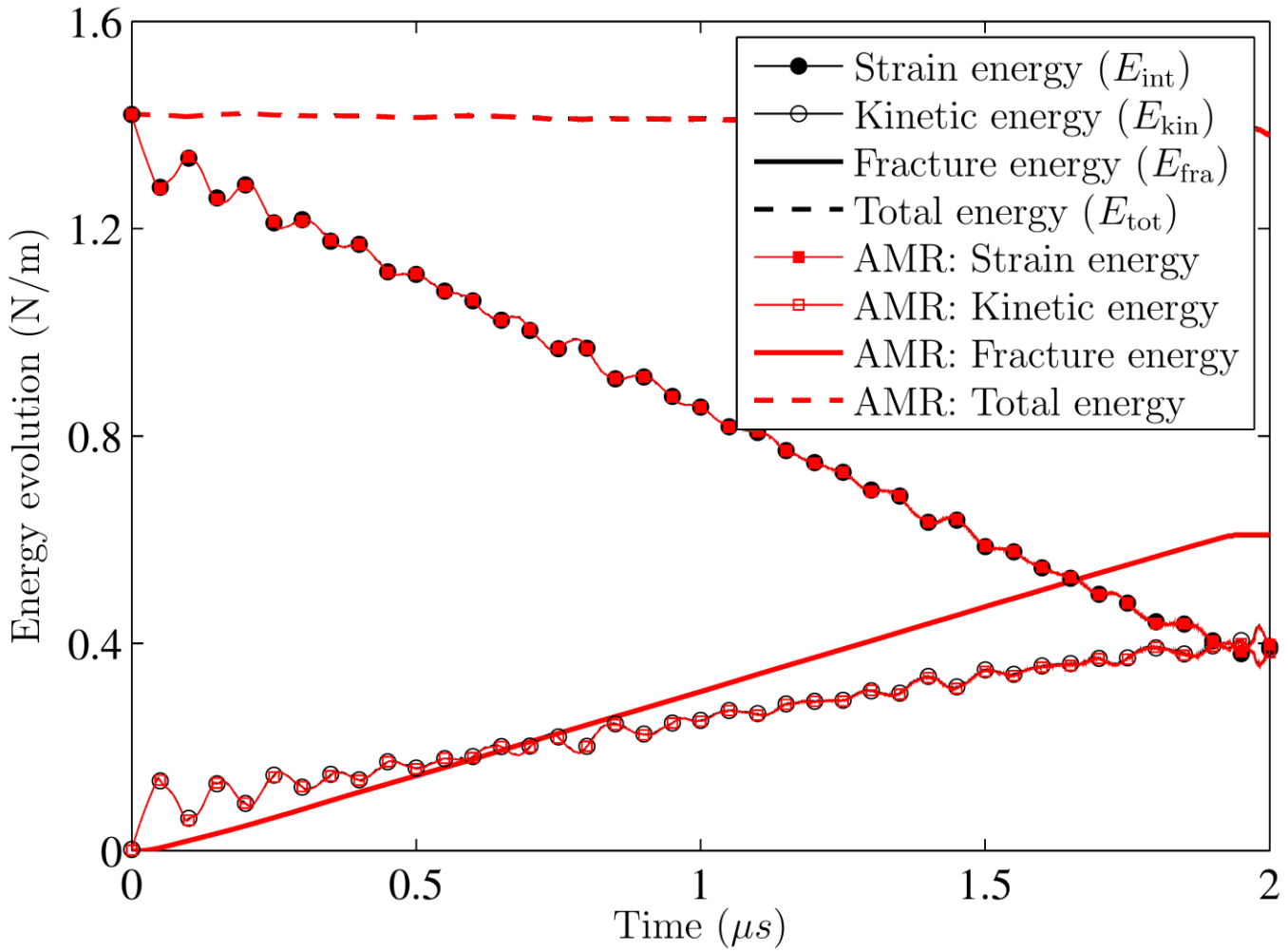

Computational Results (AMR+C)

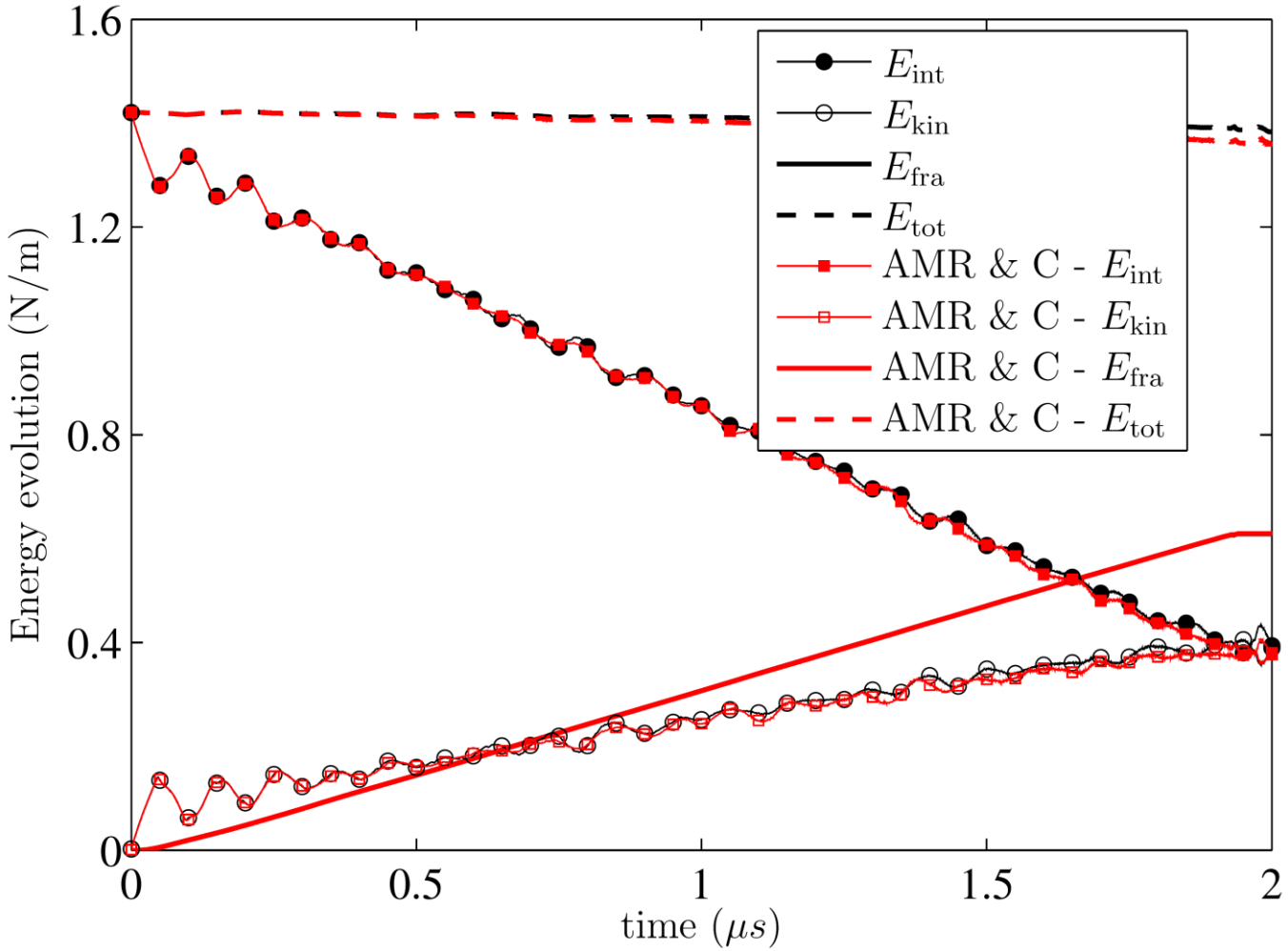

Mixed-Mode Crack Propagation

- **Kalthoff-Winkler's Experiments**

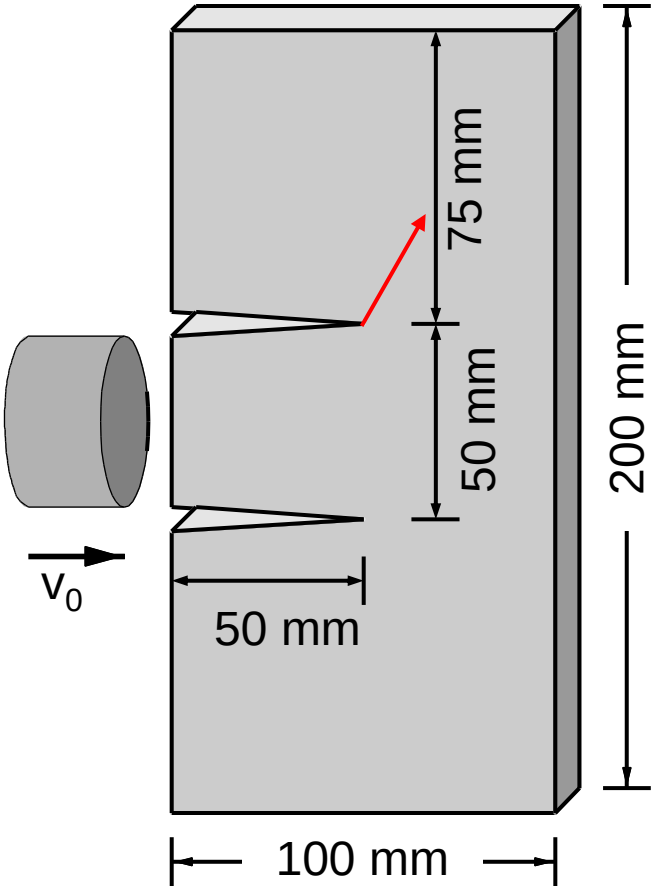

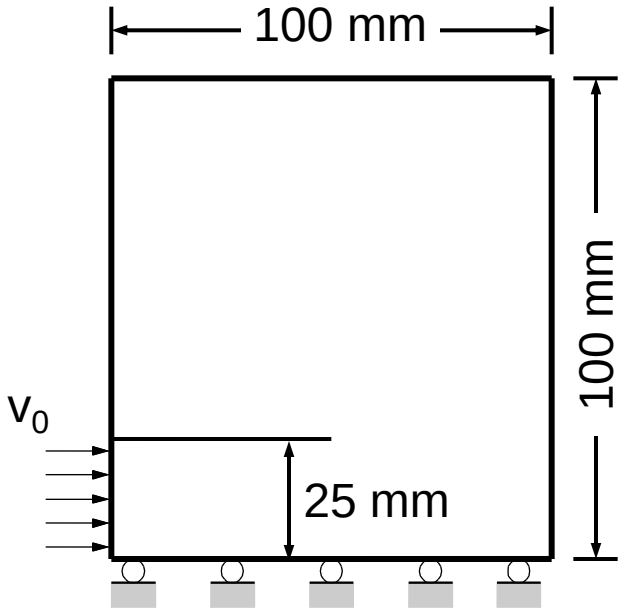

Kalthoff, J. F., Winkler, S., 1987. Failure mode transition at high rates of shear loading. International Conference on Impact Loading and Dynamic Behavior of Materials 1, 185–195.

Finite Element Mesh

- **Initial Discretization**

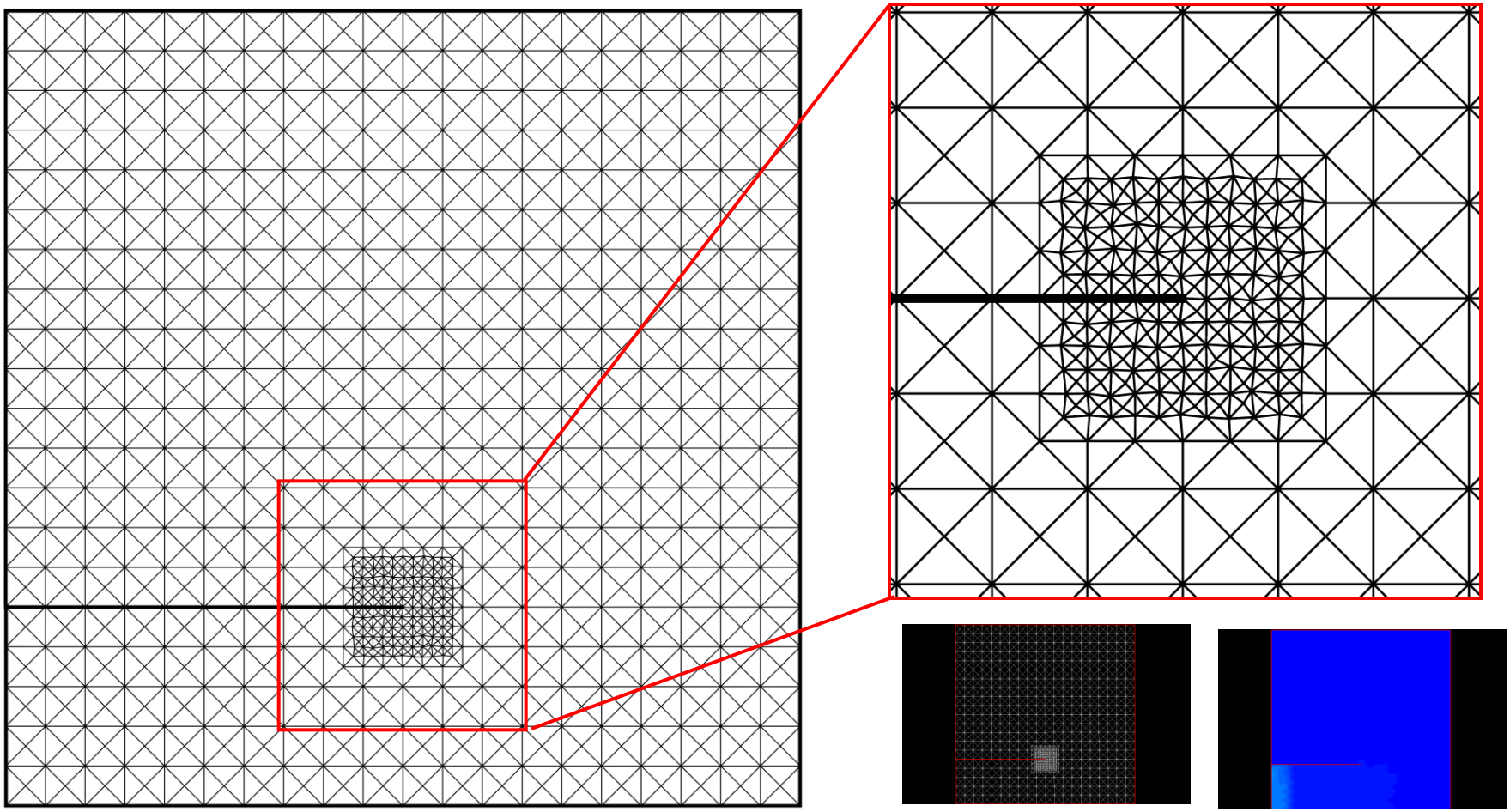

Animations (FE Mesh & Strain energy)

Computational Results

- Crack Path

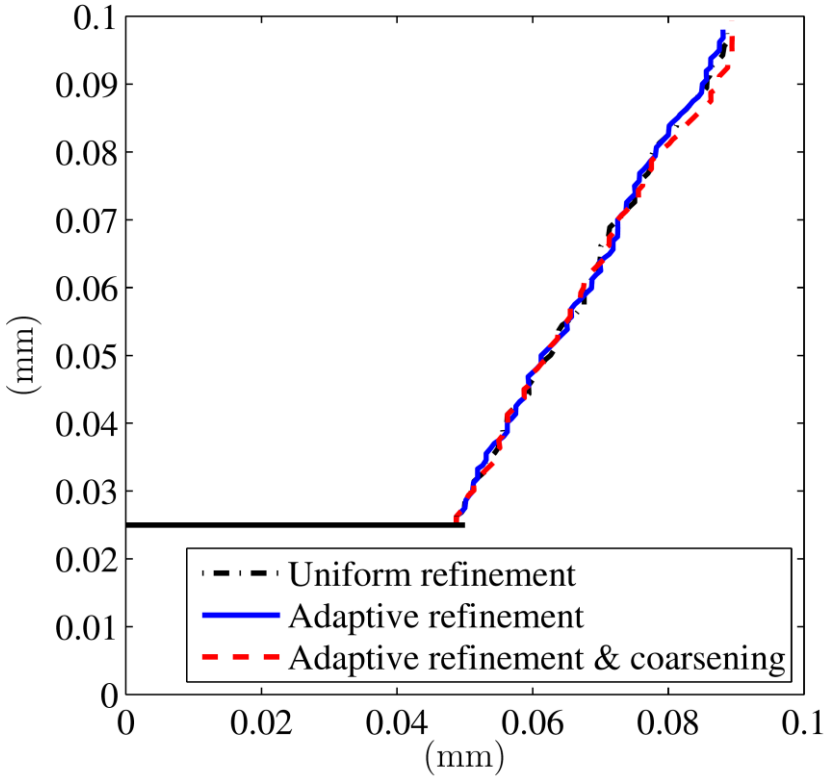

- Crack Velocity

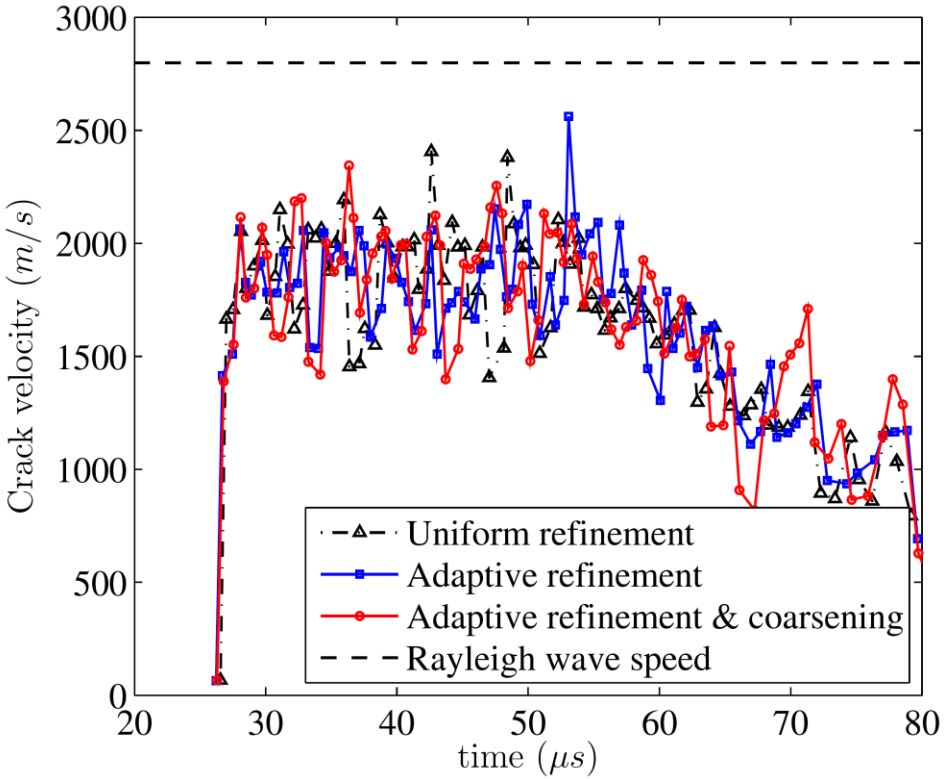

Micro-Branching Experiment

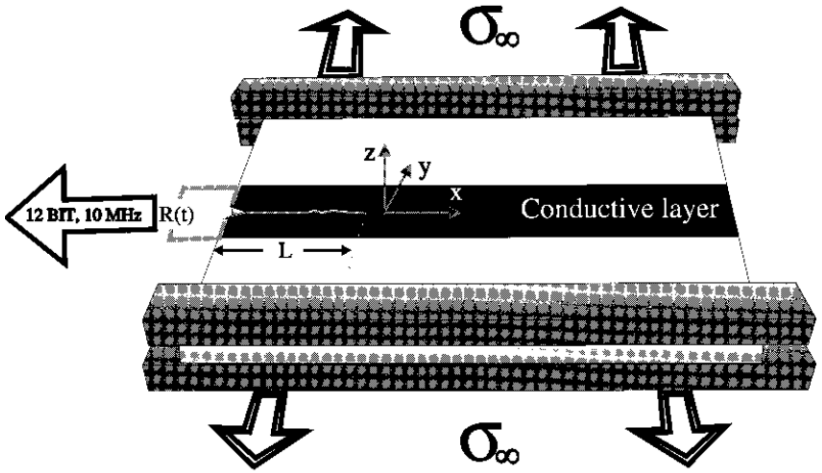

Sharon E, Fineberg J. Microbranching instability and the dynamic fracture of brittle materials. Physical Review B 1996; 54(10):7128–7139.

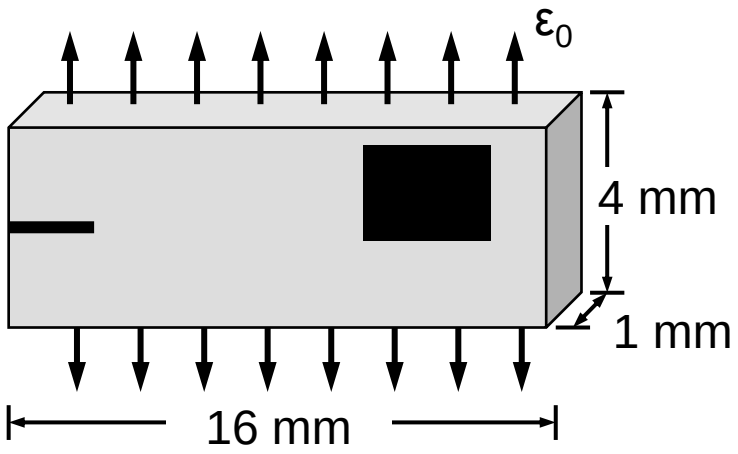

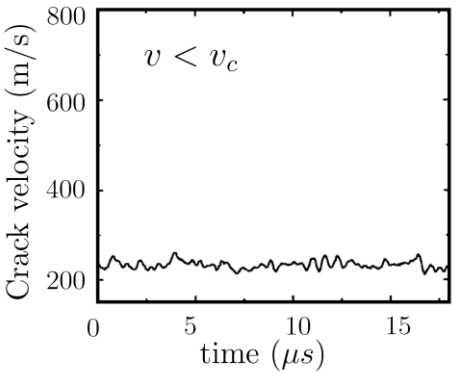

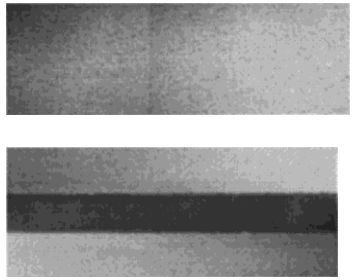

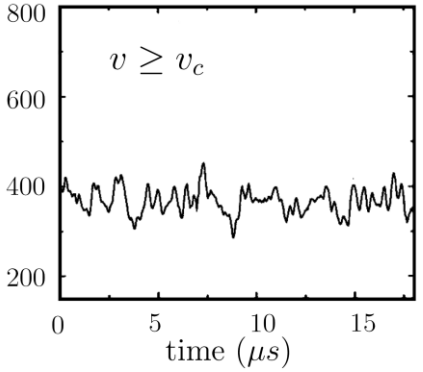

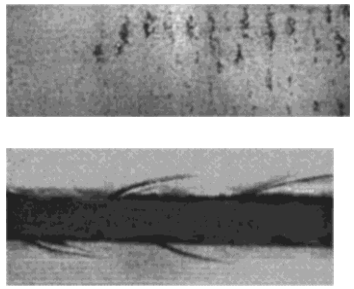

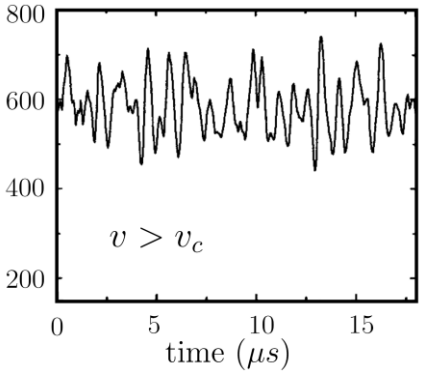

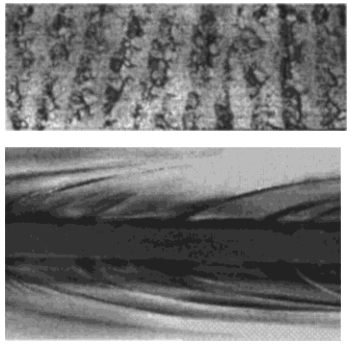

Computational Results

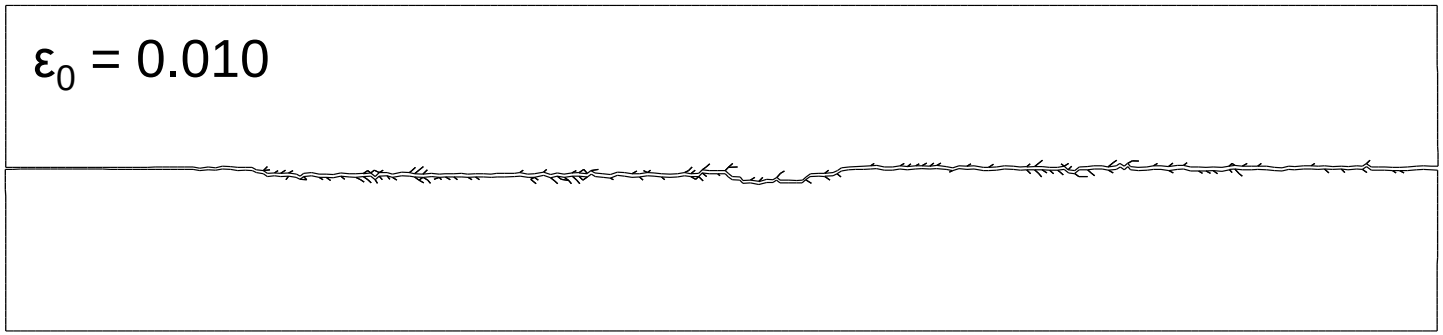

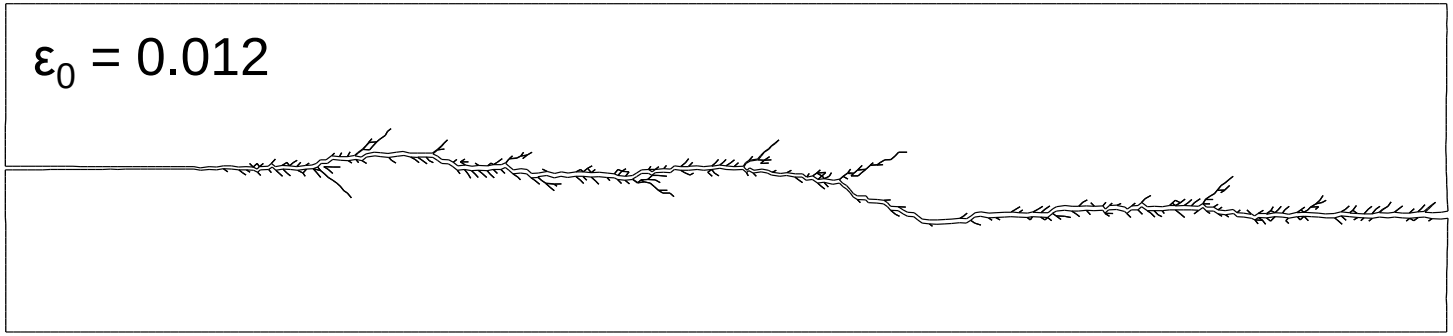

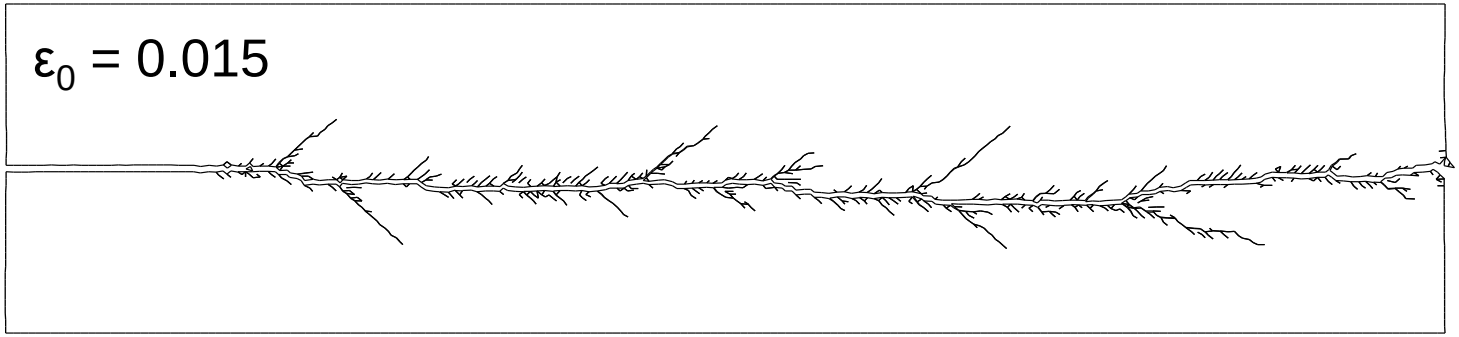

Computational Results

- **Crack Velocity**

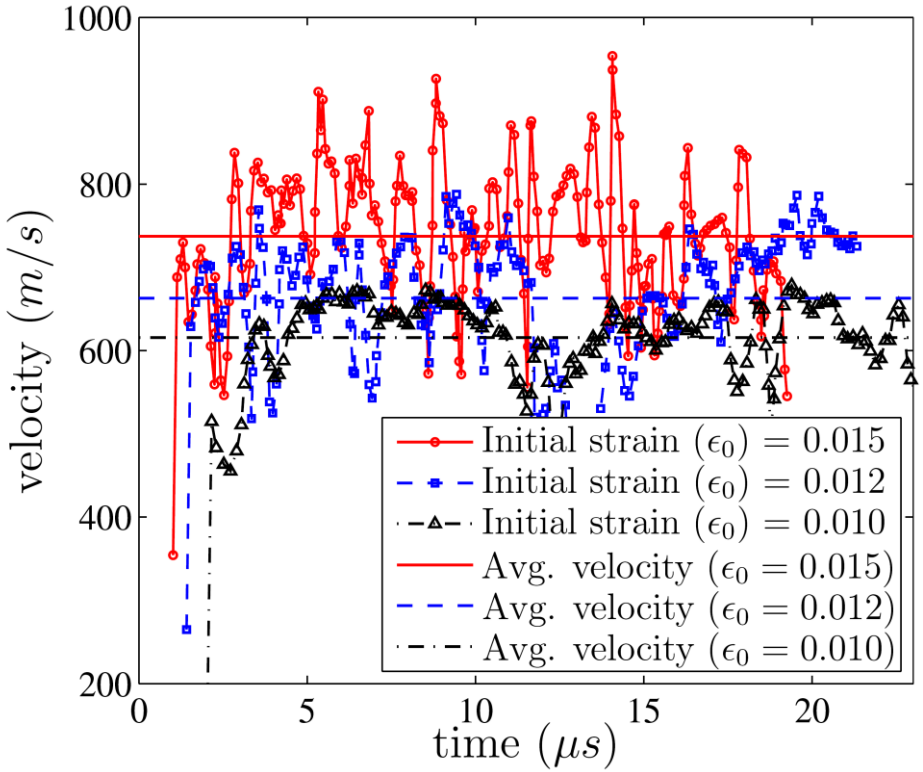

- **Energy Evolution (ε_0=0.015)**

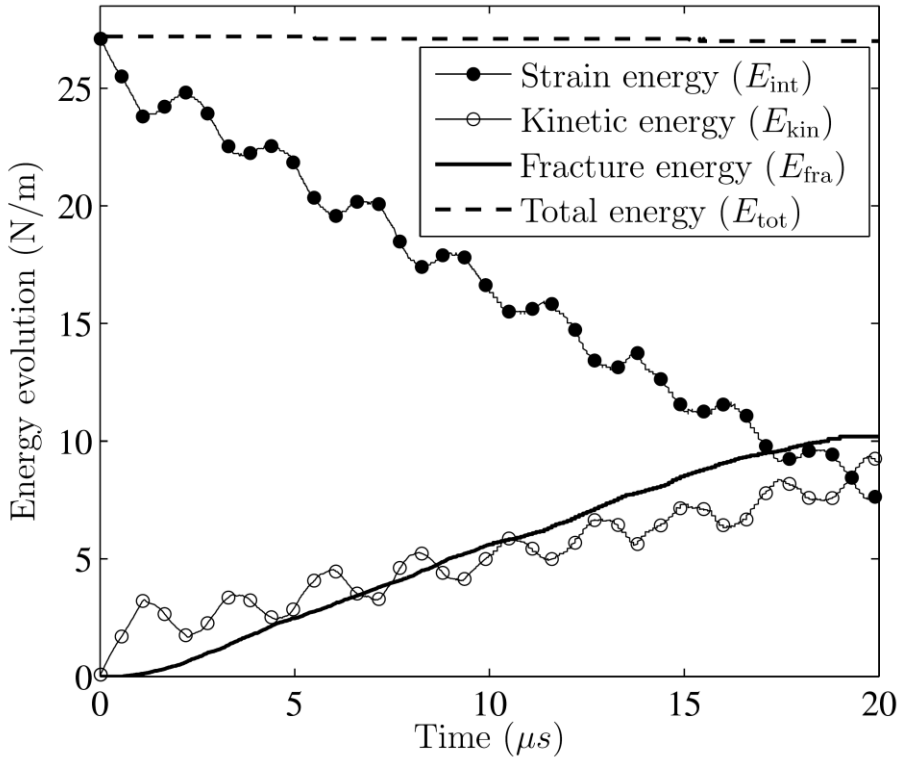

Summary

- **The potential-based constitutive model**
- **Adaptive operators**
  - Nodal perturbation, Edge-swap
  - Edge-split, Vertex-removal
- **Effective and efficient computational framework to simulate physical phenomena associated with fracture.**
- **The computational results of the adaptive mesh refinement and coarsening is consistent with the results of the uniform mesh refinement.**

QUESTIONS ?

http://ghpaulino.com